*Journal of Ceramic Processing Research. Vol. 17, No. 7, pp. 722~726 (2016)*

J O U R N A L O F
**Ceramic Processing Research**

# Mechanical synthesis and rapid consolidation of nanocrystalline TiCo-$Al_2O_3$ composites by high frequency induction heated sintering

**Jin-Kook Yoon[a] and In-Jin Shon[b,*]**
[a]*Materials Architecturing Research Center, Korea Institute of Science and Technology, PO Box 131, Cheongryang, Seoul 130-650, Korea*
[b]*Division of Advanced Materials Engineering and the Research Center of Advanced Materials Development, Engineering College, Chonbuk National University, Chonbuk 561-756, Korea*

**Despite of many attractive properties of TiCo, TiCo in industry has been limited due to low fracture toughness and a low hardness. The mechanical properties can be improved significantly by reinforcing TiCo with hard ceramic particles such as $Al_2O_3$ and by fabrication of nanostructured composite. Nanomaterials have received a good deal of attention recently as they possess high strength, high hardness, excellent ductility and toughness. In recent days, nanocrystalline powders have been developed by the thermochemical and thermomechanical process named as the spray conversion process (SCP), co-precipitation and high energy milling. Nano-powders of TiCo and $Al_2O_3$ were synthesized from $CoTiO_3$ and 2Al powders by high energy ball milling. Nanocrystalline $Al_2O_3$ reinforced composite was consolidated by high frequency induction heated sintering within one minute from mechanochemically synthesized powders of $Al_2O_3$ and TiCo. The relative density of the composite was 98%. The average hardness and fracture toughness values obtained were 1180 kg/mm$^2$ and 8.5 MPa·m$^{1/2}$, respectively.**

**Key words: Sintering, Composite, Nanomaterial, Mechanical properties, Synthesis.**

## Introduction

Intermetallic compounds have long been considered to be ideal materials destined for high temperature application in the aircraft and shuttle turbine industries. Particular attention has been paid to the TiCo, due to its high melting temperature, low density, excellent resistance to corrosion and oxidation, and high phase stability [1]. In addition, TiCo is of great interest because of shape memory properties [2]. However, like many intermetallics, use of TiCo in industry has been limited due to low fracture toughness and a low hardness. The mechanical properties can be improved significantly by reinforcing TiCo with hard ceramic particles such as $Al_2O_3$ and by fabrication of nanostructured composite [3]. Furthermore, oxidation resistance of TiCo increased with addition of $Al_2O_3$ which has a density of 3.98 g/cm$^3$, a Young's modulus of 380 GPa, excellent oxidation resistance and good high-temperature mechanical properties [4, 5]. Hence, a microstructure consisting of TiCo and $Al_2O_3$ may have sufficient oxidation resistance and mechanical properties to be a successful high temperature structural material and biomaterial.

Nanomaterials have received a good deal of attention recently as they possess high strength, high hardness, excellent ductility and toughness [6, 7]. In recent days, nanocrystalline powders have been developed by the thermochemical and thermomechanical process named as the spray conversion process (SCP), co-precipitation and high energy milling [8-10]. However, the grain size in sintered materials becomes much larger than that in pre-sintered powders due to a fast grain growth during conventional sintering process. So, controlling grain growth during sintering is one of the keys to the commercial success of nanostructured materials. In this regard, the high frequency induction heated sintering method (HFIHS) which can make dense materials within 2 min, has been shown to be effective in achieving this goal [11-13].

The purpose of this work is to produce dense nanocrystalline TiCo-$Al_2O_3$ composite within one minute from mechanically synthesized powders using high frequency induction heated sintering and to evaluate its microstructure and mechanical properties (hardness and fracture toughness).

## Experimental Procedures

Powders of 99.8% pure $CoTiO_3$ (–325 mesh, Alfa) and 99% pure Al (–325 mesh, Cerac, Inc.) were used as a starting materials. $CoTiO_3$ and 2Al powder mixtures were first milled in a high-energy ball mill, a Pulverisette-5 planetary mill, at 250 rpm for 20 hrs. Tungsten carbide balls (10 mm in diameter) were used in a sealed cylindrical stainless steel vial under an

*Corresponding author:
Tel : +82-63-270-2381
Fax: +82-63-270-2386
E-mail: ijshon@chonbuk.ac.kr

argon atmosphere. The weight ratio of ball-to-powder was 30 : 1. Milling resulted in a significant reduction in grain size.

The grain sizes of CoTi and $Al_2O_3$ were calculated by Suryanarayana and Grant Norton's formula [14],

$$B_r(B_{crystalline} + B_{strain})\cos\theta = k\lambda / L + \eta\sin\theta \qquad (1)$$

where $B_r$ is the full width at half-maximum (FWHM) of the diffraction peak after instrument correction; $B_{crystalline}$ and $B_{strain}$ are FWHM caused by small grain size and internal stress, respectively; k is constant (with a value of 0.9); $\lambda$ is the wavelength of the X-ray radiation; L and $\eta$ are grain size and internal strain, respectively; and $\theta$ is the Bragg angle. The parameters B and $B_r$ follow Cauchy's form with the relationship: $B = B_r + B_s$, where B and $B_s$ are the FWHM of the broadened Bragg peaks and the standard sample's Bragg peaks, respectively.

After milling, the mixed powders were placed in a graphite die (outside diameter, 35 mm; inside diameter, 10 mm; height, 40 mm) and then introduced into the high frequency induction heated sintering system made by Eltek in South Korea, shown schematically in Fig. 1. The four major stages in the synthesis are as follows. Stage 1-Evacuation of the system. Stage 2-Application of uniaxial pressure. Stage 3-Heating of sample by induced current. Stage 4-Cooling of sample. Temperatures were measured by a pyrometer focused on the surface of the graphite die. The process was carried out under a vacuum of 100 mtorr.

The relative densities of the sintered samples were measured by the Archimedes method. Microstructural information was obtained from product samples that were polished at room temperature. Compositional and micro structural analyses of the products were completed through X-ray diffraction (XRD) and scanning electron microscopy (SEM) with energy dispersive X-ray analysis (EDAX). Vickers hardness was measured by performing indentations at a load of 20 $kg_f$ and a dwell time of 15 s on the sintered samples.

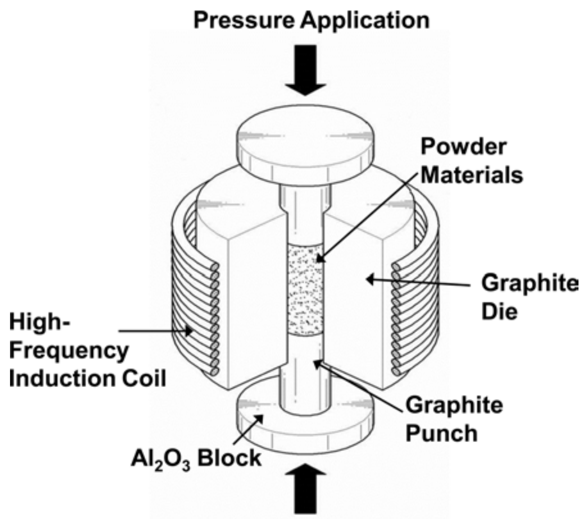


**Fig. 1.** Schematic diagram of the apparatus for high frequency induction heated sintering.

## Results and Discussion

The interaction between $TiCoO_3$ and 2Al, i.e.,

$$TiCoO_3 + 2Al \rightarrow TiCo + Al_2O_3 \qquad (2)$$

is thermodynamically feasible.

Fig. 2 shows FE-SEM images of raw powders and milled powder. The raw powders of $CoTiO_3$ and Al have irregular shape. The milled powder has some agglomeration and nano-size. X-ray diffraction results of high energy ball milled powders and raw powders are shown in Fig. 3(a), (b) and (c). The reactant

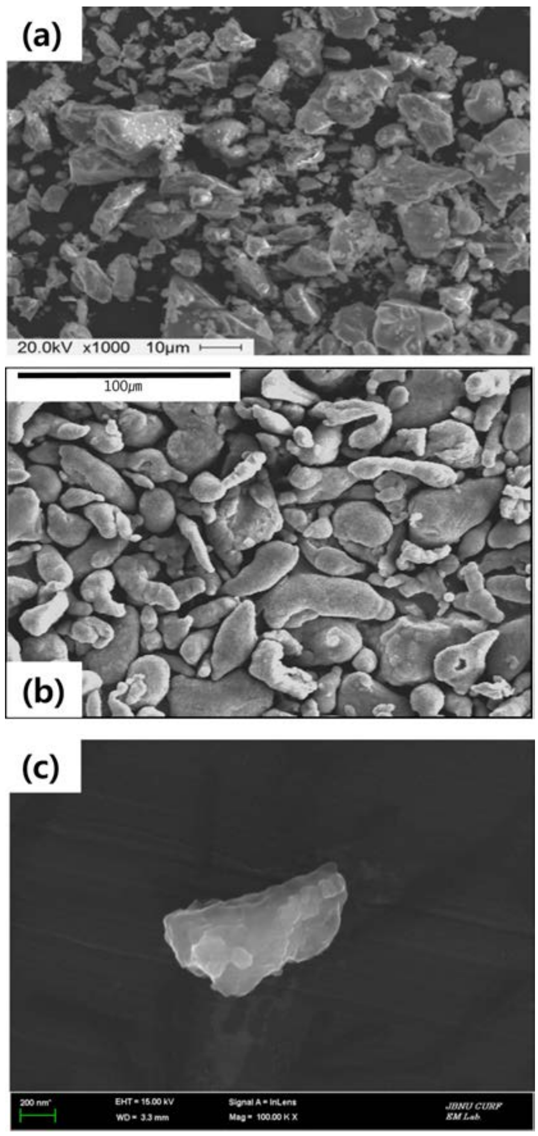


**Fig. 2.** FE-SEM images of (a) $CoTi_3$, (b) Al and (c) mechanically synthesized powder.

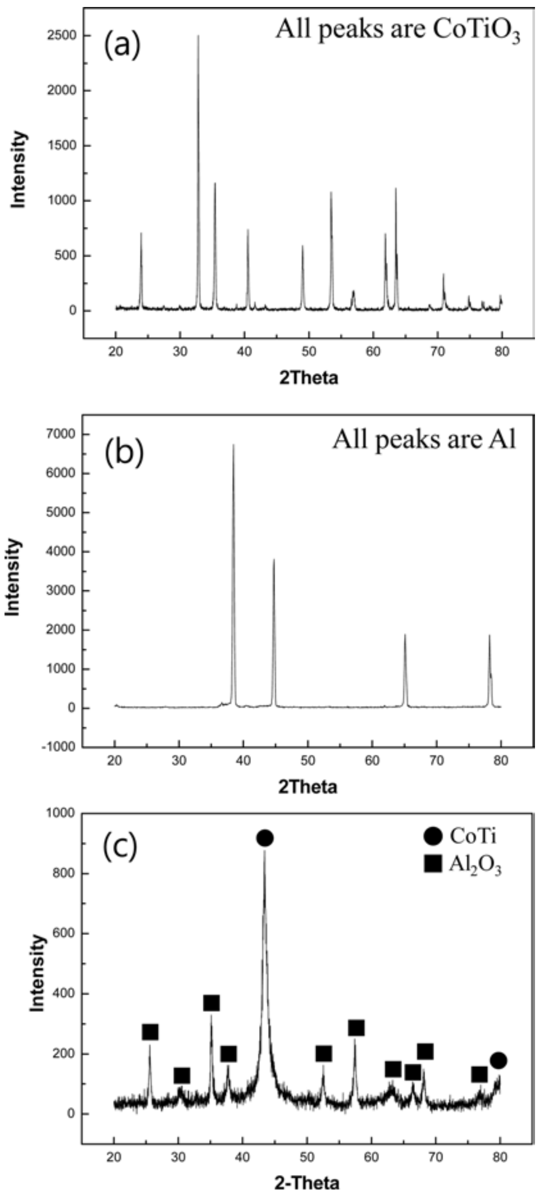


**Fig. 3.** XRD patterns of (a) $CoTi_3$, (b) Al and (c) mechanically synthesized powder.

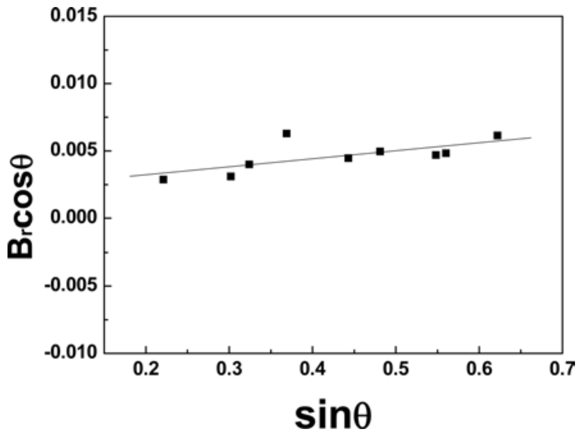


**Fig. 4.** Plot of sinè versus $B_r$cosè for $Al_2O_3$ in mechanically milled powder.

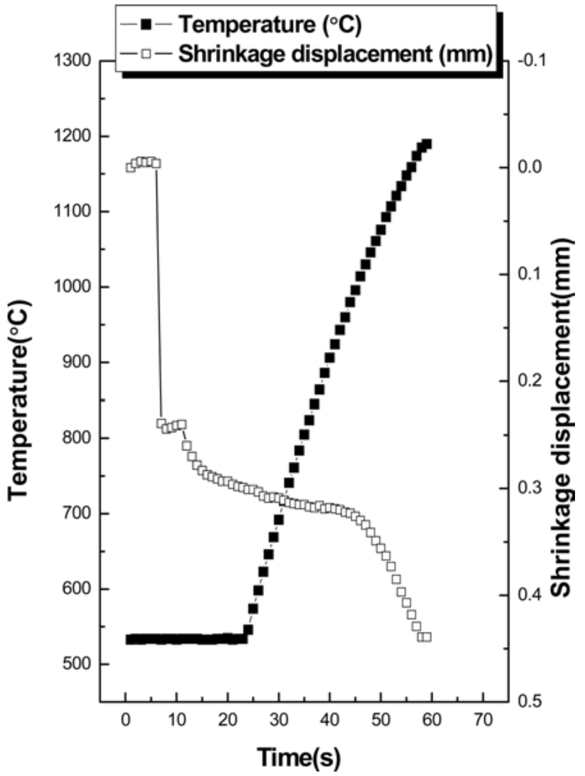


**Fig. 5.** Variation in temperature and shrinkage displacement with heating time during high frequency induction heated sintering of $TiCo$-$Al_2O_3$ systems.

powders of $TiCoO_3$ and Al were not detected in Fig. 3 (c) but products, TiCo and $Al_2O_3$, were detected. From the above result, the mechanochemical synthesis occurs completely during the high energy ball milling.

Fig. 4 shows a plot of $B_r(B_{crystalline} + B_{strain})\cos\theta$ versus sinè of $Al_2O_3$ in milled powders. The average grain sizes of $Al_2O_3$ measured by Suryanarayana and Grant Norton's formula are about 38 nm. The variations in shrinkage displacement and temperature of the surface of the graphite die with heating time during processing of TiCo and $Al_2O_3$ systems are shown Fig. 5. As the induced current was applied, the shrinkage displacement abruptly increases at heating time of 5 s and then continuously increases.

Fig. 6 shows the FE-SEM image and EDS analysis of TiCo-$Al_2O_3$ composite sintered at 1200 C. The relative density of TiCo-$Al_2O_3$ composite is about 98%. The TiCo-$Al_2O_3$ composite consists of nanocrystallites. In the figure, bright phase and dark phase are TiCo and $Al_2O_3$, respectively due to mass contrast. In EDS, Al, Ti, Co and O peaks are detected and heavier contaminants, such as W and Fe from a ball or milling container, were not detected. XRD pattern of composite sintered at 1200 °C are shown in Fig. 7. TiCo and $Al_2O_3$ peaks are detected. The structure parameters, i.e. the average grain sizes of TiCo and $Al_2O_3$ obtained from the X-ray data by Suryanarayana and Grant Norton's formula, were 95 nm and 70 nm, respectively. The average grain sizes

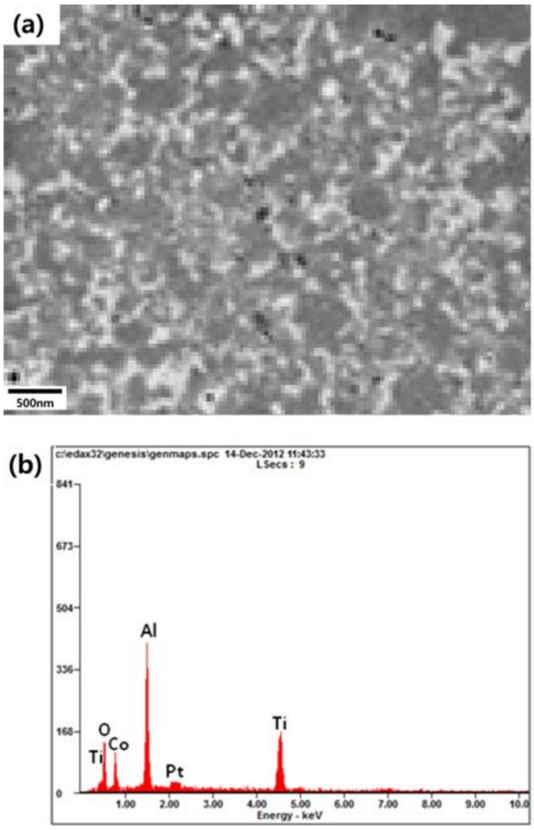


**Fig. 6.** (a) FE-SEM image and (b) EDS of TiCo-$Al_2O_3$ composite heated to 1200 °C.

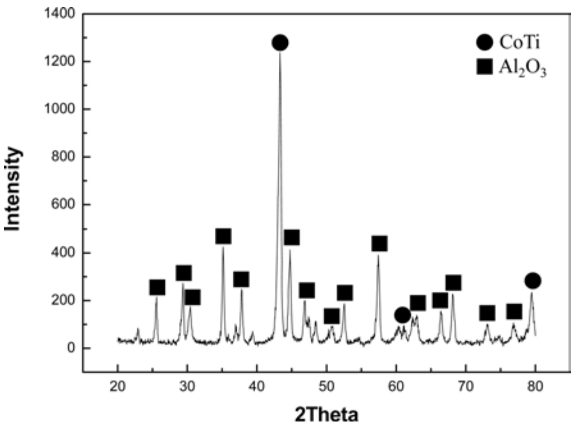


**Fig. 7.** X-ray diffraction pattern of TiCo-$Al_2O_3$ composite sintered at 1200 °C.

of the sintered TiCo and $Al_2O_3$ were not significantly larger than the grain sizes of the initial powders, indicating the absence of significant grain growth during sintering. This retention of the grain size is attributed to the high heating rate and the relatively short exposure of the powders to the high temperature. The role of current in sintering has been the focus of several attempts to explain the observed enhancement of sintering and the improved characteristics of the products. The role played by the current has been hypothesized to involve a fast heating rate due to Joule heating, the presence of plasma in pores separating

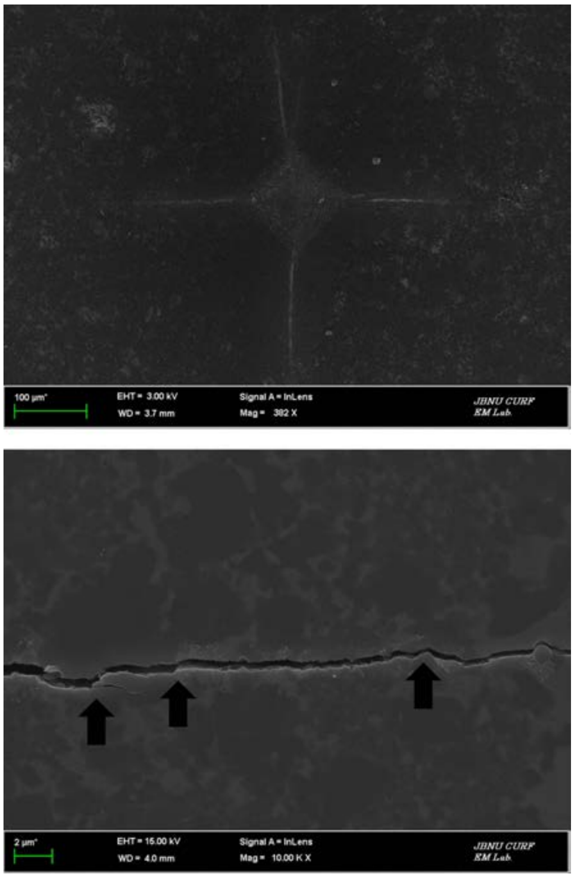

**Fig. 8.** (a) Vickers hardness indentation and (b) median crack propagation in the TiCo-$Al_2O_3$ composite.

powder particles, and the intrinsic contribution of the current to mass transport [15-18].

Vickers hardness measurements were made on polished sections of the TiCo-$Al_2O_3$ composite using a 20 $kg_f$ load and 15 s dwell time. The calculated hardness value of TiCo-$Al_2O_3$ composite was 1180 kg/mm$^2$. This value represents an average of five measurements. Indentations with large enough loads produced median cracks around the indent. From the lengths of these cracks, fracture toughness values can be determined using an expression proposed by Niihara et al. [19],

$$K_{IC} = 0.023(c/a)^{-3/2} \cdot H_v \cdot a^{1/2} \quad (3)$$

where ***c*** is the trace length of the crack measured from the center of the indentation, $a$ is one half of the average length of the two indent diagonals, and $H_v$ is the hardness.

As in the case of the hardness value, the toughness value is the average of five measurements. The toughness value obtained by the method of calculation is 8.5 MPa·m$^{1/2}$. A typical indentation pattern for the TiCo-$Al_2O_3$ composite is shown in Fig. 8(a). Typically, one to three additional cracks were observed to propagate from the indentation corner. A higher magnification view of the indentation median crack in the composite is shown in Fig. 8(b). This shows that the crack propagates in a deflective manner (↑). It is considered that TiCo and $Al_2O_3$ in the composite may deter the propagation of cracks. The hardness TiCo is reported as 750 kg/mm$^2$ [20]. The hardness of TiCo-$Al_2O_3$ composites is higher than that of monolithic TiCo due to addition of hard phase of $Al_2O_3$.

## Conclusions

Nanopowders of TiCo and $Al_2O_3$ are synthesized from $TiCoO_3$ and 2Al powders by high energy ball milling. Using the high frequency induction heated sintering method, the densification of nanocystalline $Al_2O_3$ reinforced TiCo composites were accomplished from mechanochemically synthesized powders. Complete densification can be achieved within one minute. The relative density of the composite was 98% for an applied pressure of 80 MPa and an induced current. The average grain sizes of TiCo and $Al_2O_3$ prepared by HFIHS were about 95 nm and 70 nm, respectively. The average hardness and fracture toughness values obtained were 1180 kg/mm$^2$ and 8.5 MPa·m$^{1/2}$, respectively. The hardness of TiCo-$Al_2O_3$ composites is higher than that of monolithic TiCo due to addition of hard phase of $Al_2O_3$.

## Acknowledgments

This work was supported by the KIST Institutional Program (Project No. 2E25374-15-096) and this research was supported by Basic Science Research Program though the National Research Foundation of Korea(NRF) funded by the Ministry of Education (2015R1D1A1A01056600) and this work was supported by the Korea Institute of Energy Technology Evaluation and Planning(KETEP) and the Ministry of Trade, Industry & Energy(MOTIE) of the Republic of Korea (No. 20164030201070).

## References

1. X. Wu, Intermetallics 14 (2006) 1114-1122.
2. W.L. Frankhouseser, K.W. Brendly, M.C. Kieszek, and S.T. Sullivan, Gasless Combustion Synthesis of Refractory Compounds, Noyes Publication, Park Ridge, NJ, USA, (1985).
3. A. Taotao, Chinese Journal of Aeronautics 21 (2008) 559-564.
4. Z.W. Li, W. Gao, D.L. Zhang, and Z.H. Cai, Corrosion Science 46 (2004) 1997-2007.
5. M.F. Ashby, and D.R.H. Jones, Engineering Materials 1 (International Series on Materials Science and Technology, Vol.34), Pergamon Press, Oxford, (1986).
6. K. Niihara, and A. Nikahira, Advanced structural inorganic composite, Elsevier Scientific Publishing Co., Trieste, Italy (1990).
7. I.J. Shon, H.S. Kang, J.M. Doh, and J.K. Yoon, Met. Mater. Int. 21 (2015) 345-349.
8. B.R. Kang, I.J. Shon, Korean J. Met. Mater. 53 (2015) 320-325.
9. I.J. Shon, H.G. Jo, B.S. Kim, J.K. Yoon, K.T. Hong, Korean J. Met. Mater. 53 (2015) 474-479.
10. I.J. Shon, H.G. Jo, and H.J. Kwon, Korean J. Met. Mater. 52 (2014) 343-346.
11. In-Jin Shon, Byung-Su Kim, Jin-Kook Yoon, Kyung-Tae Hong, and Na-Ra Park, Journal of Ceramic Processing Research 16 (2015) 422-427.
12. S.M. Kwon, N.R. Park, J.W. Shin, S.H. Oh, B.S. Kim, I.J. Shon, Korean J. Met. Mater. 53 (2015) 555-562.
13. I.J. Shon, Korean J. Met. Mater. 52 (2014) 573-580.
14. C. Suryanarayana, and M. Grant Norton, X-ray Diffraction: A Practical Approach, Plenum Press, New York, (1998) 213.
15. Z. Shen, M. Johnsson, Z. Zhao and M. Nygren, J. Am. Ceram. Soc. 85 (2002) 1921-1927.
16. J.E. Garay, U. Anselmi-Tamburini, Z.A. Munir, S.C. Glade, and P. Asoka-Kumar, Appl. Phys. Lett. 85 (2004) 573-575.
17. J.R. Friedman, J.E. Garay. U. Anselmi-Tamburini, and Z.A. Munir, Intermetallics 12 (2004) 589-597.
18. J.E. Garay, U. Anselmi-Tamburini, and Z.A. Munir, Acta Mater. 51 (2003) 4487-4495.
19. K. Niihara, R. Morena, and D.P.H. Hasselman, J. Mater. Sci. Lett. 1 (1982) 13-16.
20. I.J. Shon, H.S. Kang, C.Y. Suh, W. Kim. And S.W. Cho, Materials Transaction 52 (2011) 2262-2265.